Nanoselective area growth of GaN by metalorganic vapor phase epitaxy on 4H-SiC using epitaxial graphene as a mask

Renaud Puybaret, Gilles Patriarche, Matthew B. Jordan, Suresh Sundaram, Youssef El Gmili, Jean-Paul Salvestrini, Paul L. Voss, Walt A. de Heer, Claire Berger, and Abdallah Ougazzaden'

Citation: Appl. Phys. Lett. **108**, 103105 (2016); doi: 10.1063/1.4943205
View online: http://dx.doi.org/10.1063/1.4943205
View Table of Contents: http://aip.scitation.org/toc/apl/108/10
Published by the American Institute of Physics

RIGHTSLINK

Nanoselective area growth of GaN by metalorganic vapor phase epitaxy on 4H-SiC using epitaxial graphene as a mask

Renaud Puybaret,[1,2] Gilles Patriarche,[3] Matthew B. Jordan,[1,2] Suresh Sundaram,[2] Youssef El Gmili,[2] Jean-Paul Salvestrini,[4] Paul L. Voss,[1,2] Walt A. de Heer,[5] Claire Berger,[5,6] and Abdallah Ougazzaden[1,2,a)]

[1]*School of Electrical and Computer Engineering, Georgia Institute of Technology, Atlanta, Georgia 30332, USA*
[2]*CNRS UMI 2958, Georgia Institute of Technology, 2 Rue Marconi, 57070 Metz, France*
[3]*CNRS, Laboratoire de Photonique et de Nanostructures, Route de Nozay, 91460 Marcoussis, France*
[4]*Université de Lorraine, CentraleSupélec, LMOPS, EA4423, 57070 Metz, France*
[5]*School of Physics, Georgia Institute of Technology, Atlanta, Georgia 30332, USA*
[6]*CNRS, Institut Néel, BP166, 38042 Grenoble Cedex 9, France*

(Received 6 November 2015; accepted 16 February 2016; published online 9 March 2016)

We report the growth of high-quality triangular GaN nanomesas, 30-nm thick, on the C-face of 4H-SiC using nanoselective area growth (NSAG) with patterned epitaxial graphene grown on SiC as an embedded mask. NSAG alleviates the problems of defects in heteroepitaxy, and the high mobility graphene film could readily provide the back low-dissipative electrode in GaN-based optoelectronic devices. A 5–8 graphene-layer film is first grown on the C-face of 4H-SiC by confinement-controlled sublimation of silicon carbide. Graphene is then patterned and arrays of 75-nm-wide openings are etched in graphene revealing the SiC substrate. A 30-nm-thick GaN is subsequently grown by metal organic vapor phase epitaxy. GaN nanomesas grow epitaxially with perfect selectivity on SiC, in the openings patterned through graphene. The up-or-down orientation of the mesas on SiC, their triangular faceting, and cross-sectional scanning transmission electron microscopy show that they are biphasic. The core is a zinc blende monocrystal surrounded with single-crystal wurtzite. The GaN crystalline nanomesas have no threading dislocations or V-pits. This NSAG process potentially leads to integration of high-quality III-nitrides on the wafer scalable epitaxial graphene/silicon carbide platform. © *2016 AIP Publishing LLC*. [http://dx.doi.org/10.1063/1.4943205]

For the past five years, there has been much interest in integrating graphene and nitride-based semiconductors. For instance, boron nitride is used as a substrate and top gate for graphene electronics.[1–3] Aluminium nitride and silicon nitride can both serve as a mask for selective epitaxial graphene (EG) growth on silicon carbide.[4,5] Graphene is also included in InGaN/GaN optoelectronic devices as a transparent top window electrode,[6–8] or as a substrate for growth of transferable InGaN-based multi-quantum well (MQWs) light-emitting diodes (LEDs),[9,10] and even as a heat spreader.[11]

During bulk heteroepitaxy, GaN and InGaN grow with many defects,[12,13] notably threading dislocations leading to V-pits, lattice mismatch strain relaxation, and transition from 2D to 3D growth and inhomogeneous indium incorporation (for InGaN). Such defects are detrimental to optoelectronic (and electronic) device performance, as they act as non-radiative recombination centers and leakage-current paths.[14–16] Heteroepitaxial nanoselective area growth (NSAG)[12,17,18] alleviates these problems and produces high-quality and thick InGaN and GaN crystals. InGaN and GaN nanopyramids, with thickness over 100 nm and with no defects have been consistently grown with high throughput on various substrates, including silicon.[13,19,20] Difficulty with NSAG comes from the additional processing steps required to pattern the mask and remove it after the nitride growth, and to implement the device back electrodes.[7,21,22]

In this letter, we report an NSAG technique that uses multilayer epitaxial graphene (MEG) on SiC as an embedded mask, which could then be used as the back electrode to the grown GaN. This is possible because, as we show below, GaN solely grows on SiC from the holes etched through the graphene, and as it becomes thicker than the depth of the few-atomic-layer hole, it makes a recovering contact with graphene.

This process is a simple and straightforward approach for combining III-N crystals with EG on SiC. EG on SiC is an ideal platform for electronics and optoelectronics fabrication. It can be grown in large continuous films on silicon carbide,[23,24] making it a wafer-scalable technology: indeed, SiC wafers are available commercially up to 150 mm (6 in.) in diameter, and price is dropping steadily down to below 100 USD per square centimeter. Moreover, EG on SiC is a high mobility, high quality, and scalable form of graphene.[25–29] The contact between GaN over EG enables the use of the latter as a high electron mobility and high thermal conductivity back-electrode. The high electron mobility of graphene leads to higher thermal conductivity,[26] hence addressing a capital problem of large-scale integration: the dissipation of heat.[30] This makes SiC is a substrate of choice for III-nitride growth, as exemplified by the mass production of white-light LEDs using InGaN-on-SiC technology.[31]

Graphitized SiC substrates are therefore an interesting option for GaN technology. The process presented here circumvents the issue of lattice mismatch during heteroepitaxy

a)Electronic mail: aougazza@georgiatech-metz.fr

 © 2016 AIP Publishing LLC

RIGHTSLINK

by growing GaN selectively on SiC using nanoscale-patterned EG as a mask. Wurtzite GaN has a small in-plane lattice mismatch (3.5%) with hexagonal SiC and grows selectively on SiO_2-masked Si-face 6H-SiC.[12] Then, SiC and EG are compatible with high temperature MOVPE growth of the high quality GaN materials. Moreover, a selective area growth (SAG) of GaN on EG-masked SiC is a compelling device design to provide a direct electronic connection between an active optoelectronic alloy and a high-electron-mobility,[25,26,29] high-thermal-conductivity[11,32] electrode. Finally, the dual purpose of EG, both as mask for NSAG and potential back-electrode, drastically reduces the number of steps in the process, hence lowering both the cost and the environmental impact of the fabrication of nitride-based electronics and optoelectronics.

The first step in our process is the growth of graphene on the C-face of SiC by confinement-controlled sublimation (CCS) of silicon carbide.[23] The SiC wafers from Cree are 4H, on-axis, 350 μm thick. The wafer used here has a miscut of 0.16° from the $(000\bar{1})$ plane. An atomic force microscopy (AFM) image of the surface of our graphene sample shown in Fig. 1(a) confirms the presence of graphene layers, as shown by the MEG characteristic pleats. Typical characteristics in terms of pleat structure, including pleat height (1.5–2.4 nm), pleat surface density, and semi-hexagonal orientation, can be observed.[23,33] The underlying SiC step structure is clearly visible, with continuous graphene layers draped over it.

The Raman spectrum (wavelength 532 nm) in Fig. 1(b) reveals the characteristic graphene peaks. The graphene 2D and G peaks are clearly identified. The raw data (red) include the SiC contribution, which is substracted to give the signal of graphene only (blue). The 2D peak of all 5 samples measured so far can be fitted by a single Cauchy-Lorentz distribution[34] centered between 2694 and 2700 cm^{-1} and with FWHM comprised between 23 and 41 cm^{-1}. In this study, graphene thickness ranges from 5 to 8 layers, at 0.34 nm per layer (see Figs. 3–5). The D peak at 1350 cm^{-1} is barely noticeable. This indicates the low defect density in the graphene lattice.[34]

The next step in the process is to etch patterns in the graphene using the electron-beam lithography (with hydrogen silsesquioxane, HSQ, as negative resist) and oxygen plasma reactive ion etching (RIE). HSQ is then removed in buffered oxide etch (BOE). BOE, also known as buffered hydrofluoric acid, serves a dual purpose here, as it also removes the possible oxide of SiC formed during RIE. The substrate for GaN growth therefore consists of an array of 75-nm-wide openings in a continuous multilayer graphene film. Oxygen RIE, coupled with HF treatment, exposes SiC in the holes. The last step of the process is to grow 30-nm-thick GaN nanostructures by MOVPE.[35] The MOVPE growth is done at 1000 °C, 80 Torr, under full nitrogen ambient. This is harmless for the graphene pattern,[23] which maintains its characteristic pleat structure and semi-hexagonal orientation after growth as seen in Fig. 2(c). Graphene is also clearly visible in the scanning transmission electron microscopy (STEM) images in Figs. 3–5.

We observe that GaN grows only from the SiC surface in the holes, cf. Fig. 2, in the shape of equilateral-triangle

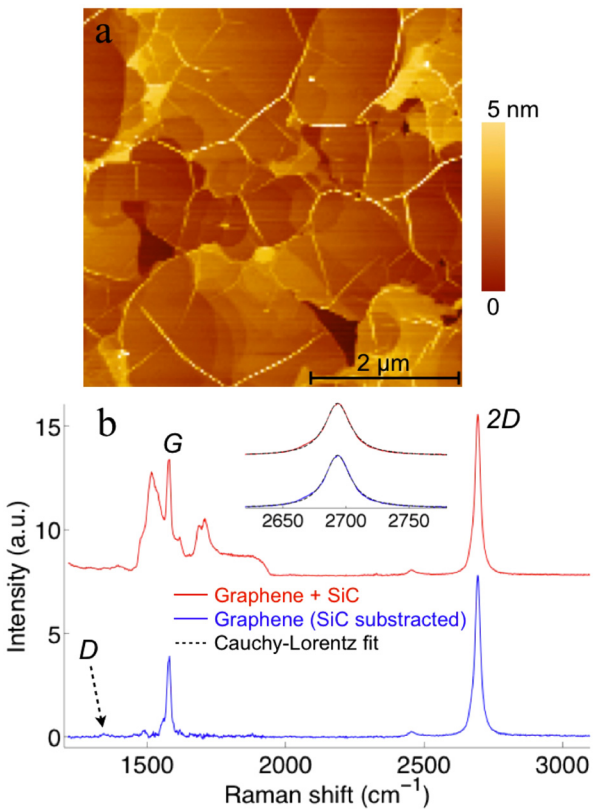

FIG. 1. After CCS graphitization of C-face SiC. (a) AFM image, $5 \times 5\ \mu m^2$. (b) Raman spectra with and without the SiC background, respectively, red and blue; the inset zooms the 2D peak.

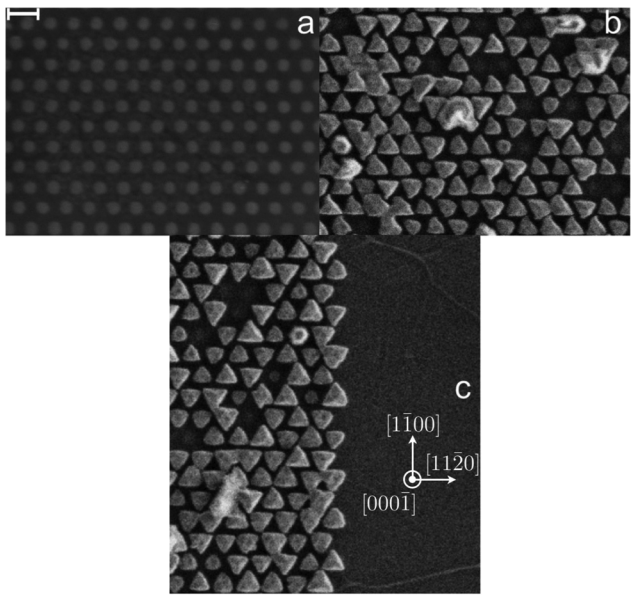

FIG. 2. Scanning electron microscope (SEM) images of NSAG of 30-nm-thick GaN on 4H-SiC C-face using EG as a mask. *Scale bar in (a) is 200* nm, *same scale in all panels*. (a) Before GaN growth, pattern of graphene (dark) on SiC (clear). (b) After MOVPE of 30 nm of GaN, GaN triangular nanomesas (clear) grow selectively in the openings revealing the SiC, and not on the graphene (dark); all the nanomesas exclusively point up or down. (c) Zoom on the edge of the mask, where we can see that GaN nucleates only on the SiC, and does not nucleate at all on the graphene, not even on the pleats: the growth is perfectly selective; *the vector basis in (c) describes the crystallographic orientations of the 4H-SiC substrate, same basis for all panels*.

RIGHTSLINK

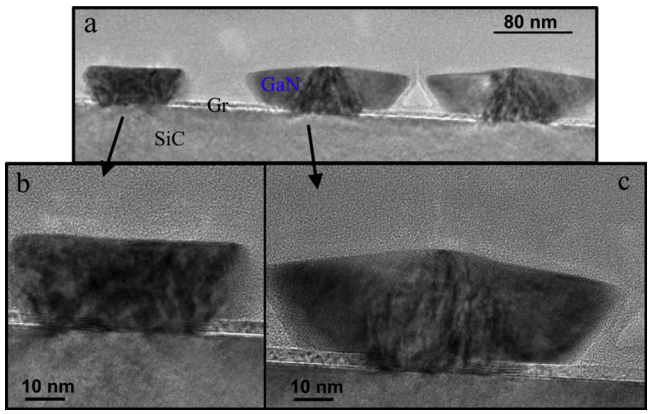

FIG. 3. Cross-sectional scanning transmission electron microscope (STEM) images: (a) 3 consecutive GaN nanomesas; (b) Zoom on the smaller left-hand nanomesa, with the flat top, having a mostly wurtzite lattice; (c) Zoom on the middle GaN nanomesa, having a large central cubic (a.k.a. zinc blende) seed on which hexagonal wurtzite facets have grown. [Note]: *A mix of surface defects and Moiré interference patterns (c-GaN and/or w-GaN and/or graphene) can seen in (b) and (c): these imagery artifacts are due to the focused ion beam (FIB) cut necessary for STEM preparation; in particular, the graphene is completely etched in the hole: the FIB sliver is wider than the hole in the graphene (70 nm); hence, the graphene behind the hole is imaged by the STEM and overlaps with the c-GaN and/or w-GaN, forming Moiré interference fringes.*[39,40]

nanomesas with no nucleation on EG. As the GaN nanomesas grows out of the SiC hole, the GaN wurtzite phase nucleates on the GaN central cubic seed (itself nucleated on the SiC revealed in the hole etched in the graphene), allowing for a small overlap of GaN on top of EG, see Figs. 3 and 5. We find that the GaN nanostructures on SiC are significantly different from the typical hexagonal nanopyramids and their six $(1\bar{1}01)$ or $(1\bar{1}02)$ r-plane facets.[12,13,19,20] Here, we use

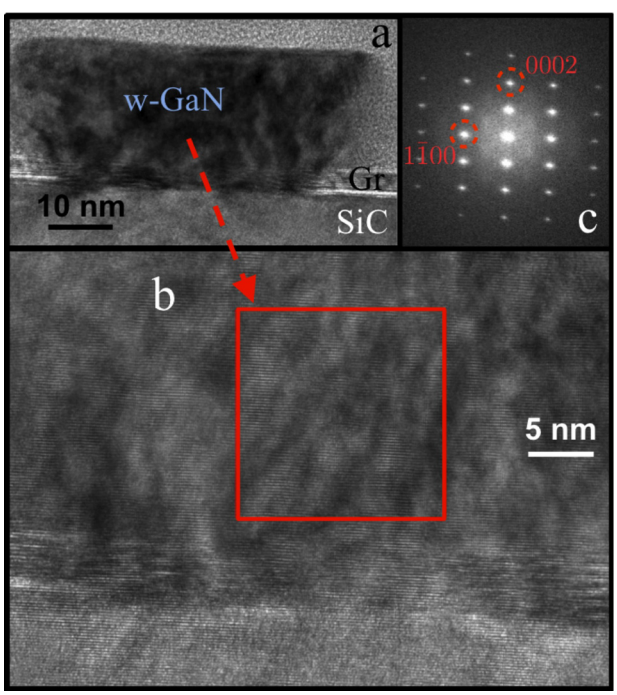

FIG. 4. Single-crystal wurtzite GaN nanomesa: (a) STEM image. (b) Zoom and definition of the zone (red square) taken for fast Fourier transform (FFT); *see [Note] on Fig. 3*. (c) FFT diffraction pattern of the area in the red box showing wurtzite GaN; *local intensity maxima 0002 and* $1\bar{1}00$ *make an angle of* **90°** *relative to the origin, characteristic of the wurtzite lattice.*

the nonwetting property of graphene, which is an advantage. The fact that coatings do not stick to graphene is in general problematic for device fabrication and nanoelectronics processing.[36,37]

The cross-section STEM images of GaN nanomesas (see Fig. 3) clearly show that the growth of GaN does not emerge from the EG patterns. The single orientation and faceting of the GaN nanomesas in Figs. 2 and 3 confirms the epitaxial growth of GaN on SiC. The vast majority (four fifths) of the GaN nanomesas has a large central triangular cubic seed, above which the hexagonal wurtzite facets have grown. These mesas are the larger ones with a roof-shaped top, as shown in Figs. 3(c) and 5. A clear evidence of each crystal phase is given by the fast Fourier transform (FFT) diffraction patterns of the observed atomic arrangements.[18,38] The wurtzite facets start growing at the edge of the SiC holes, where the graphene is present. GaN makes an overlaying contact with EG, enabling its potential use as a heat-dissipating back-electrode. The remaining fifth of the GaN nanomesas is smaller and flat-topped (cf. Figs. 3(b) and 4), and is mostly wurtzite. The evidence of their hexagonal crystal phase is given in Fig. 4(b). The very first layers of growth are cubic, as evidenced by their triangular faceting, which indicate a non-hexagonal symmetry: indeed, they do not grow as six-faceted nanopyramids as in Refs. 12,13,19, and 20. The very good uniformity of every GaN nanomesa and the absence of threading dislocation emerging from the interface with SiC are all apparent. An immediate consequence is the absence of V-pits, which normally emerge from the threading dislocations.[14,15]

The STEM analysis of the bigger GaN nanomesas, with large cubic central seed and out-growing wurtzite facets, in Fig. 5 clearly shows that cubic GaN (c-GaN) grows along the [111] direction of the underlying 4H-SiC C-face. Then, a transition region of a few atomic layers can be noticed in the high-angle annular dark field image, see Fig. 5(e): this intermediate zone, 2–3 nm from the edge of the SiC nano-hole, is a mix between both the cubic and wurtzite phases, leading to a very thin and localized structure with stacking faults in an otherwise defect-free GaN nanomesa. Finally, at the edge of the SiC hole, right where graphene has not been etched away, GaN begins wurtzite growth, see Figs. 5(d) and 5(e), with its own [0001] direction normal to the $(\bar{1}11)$ plane of the underlying c-GaN seed, illustrating the following equivalence of lattice parameters: $d\{111\}_{cubic} = d\{0002\}_{wurtzite}$.

However, one fifth of the nanomesas seems to be fully hexagonal but are still triangular-shaped, similar to the larger nanomesas, instead of exhibiting the typical hexagon-base pyramidal shape and its six $(1\bar{1}01)$ or $(1\bar{1}02)$ r-plane facets.[12,13,19,20] An explanation is that the very first few atomic layers of GaN have a cubic structure, with a quick transition to growth of the wurtzite phase. The full STEM analysis in Fig. 5 also gives insight that can explain why each GaN nanomesa on the SEM in Figs. 2(b) and 2(c) points up or down: the three (111) facets of the cubic phase grow along their three corresponding {111} axes, of which normal projections on the substrate plane are the three {110} directions. At the very beginning of growth, c-GaN conforms to the underlying 4H-SiC, hence aligning its {110} axes with the $\{11\bar{2}0\}$ of 4H-SiC.

RIGHTSLINK

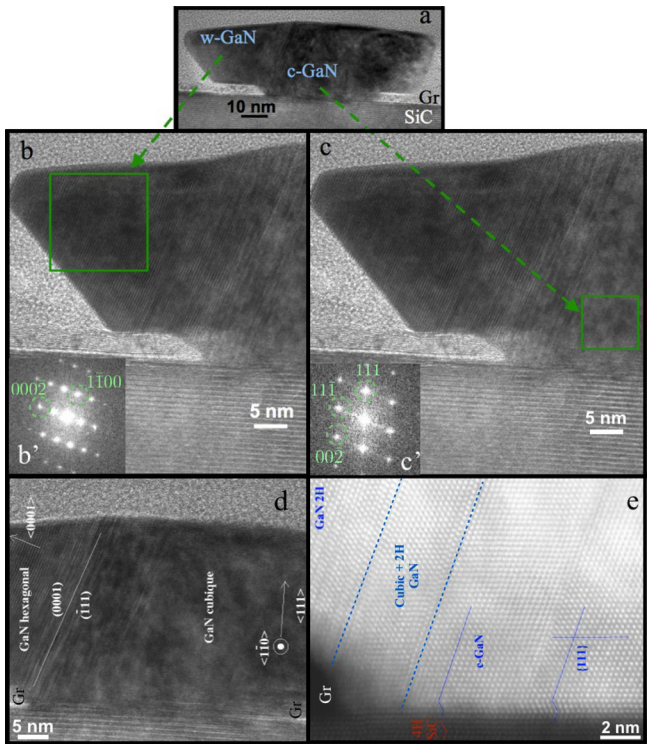

FIG. 5. GaN nanomesa with central cubic seed, and hexagonal facets (*see [Note] on Fig. 3*): (a) Cross-sectional STEM image; (b) Zoom and definition of the wurtzite zone (green box) taken for FFT and (b′) FFT diffraction pattern of the area in the green box showing wurtzite GaN. (c) Zoom and definition of the cubic zone (green box) taken for fast Fourier transform (FFT) and (c′) FFT diffraction pattern of the area in the green box showing c-GaN, where $1\bar{1}0$ faces the reader; *local intensity maxima 111 and* $11\bar{1}$ *make an angle of* **70.5**° *relative to the origin, characteristic of the zinc-blende/cubic lattice*. (d) STEM analysis and crystallographic directions. (e) Zoom on the SiC/GaN interface in the vicinity of the EG mask, high-angle annular dark field (HAADF) detector, showing both cubic and wurtzite phases on GaN, as well as the biphasic transition region; *the visible atoms are Ga in GaN and Si in SiC*.

Triangles point up or down depending on whether the $(\bar{1}11)$ plane of c-GaN makes an angle of $+70.5°$ or $-70.5°$ with the (111) plane, allowing both possible ABC or ACB chiralities of c-GaN to grow. Then, the hexagonal phases start growing out of the cubic $(\bar{1}11)$-faceted seeds, resulting, when seen from above with the SEM in Fig. 2, in north-pointing triangles when a $(\bar{1}11)$ cubic facet is facing north, and south-pointing triangles when a $(\bar{1}11)$ cubic facet is facing south. The fact that graphene mask is extremely thin (1.7 to 2.7 nm) compared to the typically used 100 nm of SiO_2 might also play a role at the beginning of growth. 4H-SiC polarity (Si- or C-face), mask thickness, and hole pattern geometry are also factors to be considered for further study.

To conclude, we have found that graphene can be used as a mask for NSAG of III-nitrides. This process is repeatable and compatible with the standard large-scale industrial electronics fabrication techniques. We show that a high-quality III-N material, with no threading dislocation, can be grown directly in contact of SiC using large continuous films of patterned epitaxial graphene as a mask. The recovering of GaN over EG could enable the dual use of graphene as a high-electron-mobility and high-thermal-conductivity back-electrode. Moreover, the technology presented here is fully developed on industry-grade and wafer-scalable SiC. The study also provides insight on the nucleation of the zinc-blende (non-polar) and wurtzite (polar) phases of GaN on 4H-SiC. At last, this process greatly simplifies NSAG with the potential dual use of MEG. We are confident that a better discrimination between the zinc blende (non-polar, 3.2 eV band gap at room temperature[41]) and wurtzite (polar, 3.4 eV at room temperature[41]) phases can be achieved through further experiments on the MOVPE conditions, graphene thickness, and mask geometry. We believe this will open direct integration of the high-quality III-nitrides with the graphene-on-SiC electronics, e.g., in terms of optoelectronic and high-frequency applications.

The authors thank the French Lorraine Region, the National Science Foundation (Grant NSF-ECCS No. 1506006), the Air Force Office of Scientific Research (contract FA9550-13-1-0217), the Partner University Fund, the Graphene Flagship EU Grant No. 604391, the French National Research Agency (ANR), under the NOVAGAINS Project (ANR-12-PRGE-0014-02), and CNRS INCEPT PEPS Project.

[1]G. Giovannetti, P. A. Khomyakov, G. Brocks, P. J. Kelly, and J. van den Brink, Phys. Rev. B **76**, 073103 (2007).
[2]C. R. Dean, A. F. Young, I. Meric, C. Lee, L. Wang, S. Sorgenfrei, K. Watanabe, T. Taniguchi, P. Kim, K. L. Shepard, and J. Hone, Nat. Nanotechnol. **5**, 722–726 (2010).
[3]A. S. Mayorov, R. V. Gorbachev, S. V. Morozov, L. Britnell, R. Jalil, L. A. Ponomarenko, P. Blake, K. S. Novoselov, K. Watanabe, T. Taniguchi, and A. K. Geim, Nano Lett. **11**, 2396–2399 (2011).
[4]M. Rubio-Roy, F. Zaman, Y. Hu, C. Berger, M. W. Moseley, J. D. Meindl, and W. A. de Heer, Appl. Phys. Lett. **96**, 082112 (2010).
[5]R. Puybaret, J. Hankinson, J. Palmer, C. Bouvier, A. Ougazzaden, P. L. Voss, C. Berger, and W. A. de Heer, J. Phys. D: Appl. Phys. **48**, 152001 (2015); e-print arXiv:13076197.
[6]G. Jo, M. Choe, C. Y. Cho, J. H. Kim, W. Park, S. Lee, W. K. Hong, T. W. Kim, S. J. Park, B. H. Hong, Y. H. Kahng, and T. Lee, Nanotechnology **21**, 175201 (2010).
[7]D. W. Jeon, W. M. Choi, H. J. Shin, S. M. Yoon, J. Y. Choi, L. W. Jang, and I. H. Lee, J. Mater. Chem. **21**(44), 17688–17692 (2011).
[8]B. J. Kim, C. Lee, Y. Jung, K. H. Baik, M. A. Mastro, J. K. Hite, C. R. Eddy, Jr., and J. Kim, Appl. Phys. Lett. **99**, 143101 (2011).
[9]K. Chung, C. H. Lee, and G. C. Yi, Science **330**, 655–657 (2010).
[10]J. Kim, C. Bayram, H. Park, C. W. Cheng, C. Dimitrakopoulos, J. A. Ott, K. B. Reuter, S. W. Bedell, and D. K. Sadana, Nat. Commun. **5**, 4836 (2014).
[11]N. Han, T. V. Cuong, M. Han, B. D. Ryu, S. Chandramohan, J. B. Park, J. H. Kang, Y. J. Park, K. B. Ko, H. Y. Kim, H. K. Kim, J. H. Ryu, Y. S. Katharria, C. J. Choi, and C. H. Hong, Nat. Commun. **4**, 1452 (2013).
[12]W. H. Goh, J. Martin, S. Ould-Saad, S. Gautier, A. A. Sirenko, A. Martinez, L. Le Gratiet, A. Ramdane, N. Maloufi, and A. Ougazzaden, Phys. Status Solidi C **6**, S510–S513 (2009).
[13]S. Sundaram, Y. El Gmili, R. Puybaret, X. Li, P. L. Bonanno, K. Pantzas, G. Patriarche, P. L. Voss, J. P. Salvestrini, and A. Ougazzaden, Appl. Phys. Lett. **107**, 113105 (2015).
[14]B. Heying, X. H. Wu, S. Keller, Y. Li, D. Kapolnek, B. P. Keller, S. P. DenBaars, and J. S. Speck, Appl. Phys. Lett. **68**, 643–645 (1996).
[15]X. H. Wu, C. R. Elsass, A. Abare, M. Mack, S. Keller, P. M. Petroff, S. P. DenBaars, J. S. Speck, and S. J. Rosner, Appl. Phys. Lett. **72**, 692–694 (1998).
[16]S. Nakamura, S. Pearton, and G. Fasol, *The Blue Laser Diode: The Complete Story* (Springer, 2000).
[17]D. Zubia and S. D. Hersee, J. Appl. Phys. **85**, 6492–6496 (1999).
[18]X. Y. Sun, R. Bommena, D. Burckel, A. Frauenglass, M. N. Fairchild, S. R. J. Brueck, G. A. Garrett, M. Wraback, and S. D. Hersee, J. Appl. Phys. **95**, 1450–1454 (2004).
[19]S. Sundaram, R. Puybaret, Y. El Gmili, X. Li, P. L. Bonanno, K. Pantzas, G. Orsal, D. Troadec, Z. H. Cai, G. Patriarche, P. L. Voss, J. P. Salvestrini, and A. Ougazzaden, J. Appl. Phys. **116**, 163105 (2014).

RIGHTSLINK

[20]S. Sundaram, R. Puybaret, X. Li, Y. El Gmili, J. Streque, K. Pantzas, G. Orsal, G. Patriarche, P. L. Voss, J. P. Salvestrini, and A. Ougazzaden, Phys. Status Solidi A **212**, 740 (2015).
[21]J. Kang, Z. Li, H. Li, Z. Liu, X. Li, X. Yi, P. Ma, H. Zhu, and G. Wang, Appl. Phys. Express **6**, 072102 (2013).
[22]C. Y. Chang, H. Li, K. B. Hong, Y. Y. Yang, W. C. Lai, and T. C. Lu, Superlattices Microstruct. **86**, 275–279 (2015).
[23]W. de Heer, C. Berger, M. Ruan, M. Sprinkle, X. Li, Y. Hu, B. Zhang, J. Hankinson, and E. Conrad, Proc. Natl. Acad. Sci. **108**, 16900–16905 (2011).
[24]J. Palmer, J. Kunc, Y. Hu, J. Hankinson, Z. Guo, C. Berger, and W. A. de Heer, Appl. Phys. Lett. **105**, 023106 (2014).
[25]C. Berger, Z. Song, T. Li, X. Li, A. Ogbazghi, R. Feng, Z. Dai, A. Marchenkov, E. Conrad, P. First, and W. de Heer, J. Phys. Chem. B **108**, 19912–19916 (2004).
[26]C. Berger, Z. Song, X. Li, X. Wu, N. Brown, C. Naud, D. Mayou, T. Li, J. Hass, A. Marchenkov, E. Conrad, P. First, and W. A. de Heer, Science **312**, 1191–1196 (2006).
[27]M. Sprinkle, M. Ruan, Y. Hu, J. Hankinson, M. Rubio-Roy, B. Zhang, X. Wu, C. Berger, and W. A. de Heer, Nat. Nanotechnol. **5**, 727–731 (2010).
[28]K. S. Novoselov, V. I. Fal'ko, L. Colombo, P. R. Gellert, M. G. Schwab, and K. Kim, Nature **490**, 192–200 (2012).
[29]J. Baringhaus, M. Ruan, F. Edler, A. Tejeda, M. Sicot, A. Taleb-Ibrahimi, A. P. Li, Z. Jiang, E. H. Conrad, C. Berger, C. Tegenkamp, and W. A. de Heer, Nature **506**, 349–354 (2014).
[30]P. Gelsinger, *Computer Power User Magazine* (Intel Developer Forum, 2004).
[31]K. M. Doverspike, J. A. Edmond, H.-S. Kong, H. M. Dieringer, and D. B. Slater, Jr., "Vertical geometry InGaN LED," U.S. patent 6,459,100 (16 September 1998).
[32]A. A. Balandin, S. Ghosh, W. Bao, I. Calizo, D. Teweldebrhan, F. Miao, and C. N. Lau, Nano Lett. **8**, 902–907 (2008).
[33]Y. Hu, M. Ruan, Z. Guo, R. Dong, J. Palmer, J. Hankinson, C. Berger, and W. A. de Heer, J. Phys. D: Appl. Phys. **45**, 154010 (2012).
[34]C. Faugeras, A. Nerriere, M. Potemski, A. Mahmood, E. Dujardin, C. Berger, and W. A. de Heer, Appl. Phys. Lett. **92**, 011914 (2008).
[35]J. Martin, A. Martinez, W. H. Goh, S. Gautier, N. Dupuis, L. Le Gratiet, J. Decobert, A. Ramdane, N. Maloufi, and A. Ougazzaden, Mater. Sci. Eng. B **147**, 114 (2008).
[36]Z. Guo, R. Dong, P. S. Chakraborty, N. Lourenco, J. Palmer, Y. Hu, M. Ruan, J. Hankinson, J. Kunc, J. D. Cressler, C. Berger, and W. A. de Heer, Nano Lett. **13**, 942–947 (2013).
[37]R. Dong, Z. Guo, J. Palmer, Y. Hu, M. Ruan, J. Hankinson, J. Kunc, S. K. Bhattacharya, C. Berger, and W. A. de Heer, J. Phys. D: Appl. Phys. **47**, 094001 (2014).
[38]C. Bayram, J. A. Ott, K. T. Shiu, C. W. Cheng, Y. Zhu, J. Kim, M. Razeghi, and D. K. Sadana, Adv. Funct. Mater. **24**, 4491 (2014).
[39]L. Lechner, J. Biskupek, and U. Kaiser, Microsc. Microanal. **17**, 628–629 (2011).
[40]S. K. Boda, G. Thrivikraman, and B. Basu, J. Mater. Chem. B **3**, 3150–3168 (2015).
[41]V. Bougrov, M. E. Levinshtein, S. L. Rumyantsev, and M. S. Shur, *Properties of Advanced Semiconductor Materials: GaN, AlN, InN, BN, SiC, SiGe* (John Wiley & Sons, 2001).

RIGHTSLINK